Materials Today Bio 28 (2024) 101187

Contents lists available at ScienceDirect

Materials Today Bio

journal homepage: www.journals.elsevier.com/materials-today-bio

Silica 3D printed scaffolds as pH stimuli-responsive drug release platform

Raquel Rodríguez-González [a,b], José Ángel Delgado [a], Luis M. Delgado [a,b,*], Román A. Pérez [a,b,**]

[a] Bioengineering Institute of Technology (BIT), Universitat Internacional de Catalunya (UIC), Barcelona, 08017, Spain
[b] Basic Sciences Department, Faculty of Medicine and Health Sciences, Universitat Internacional de Catalunya, Barcelona, Spain

ARTICLE INFO

Keywords:
Silica sol-gel
3D printing
Bioactivity
pH-sensitive
Stimuli-responsive
Drug delivery systems

ABSTRACT

Silica-based scaffolds are promising in Tissue Engineering by enabling personalized scaffolds, boosting exceptional bioactivity and osteogenic characteristics. Moreover, silica materials are highly tunable, allowing for controlled drug release to enhance tissue regeneration. In this study, we developed a 3D printable silica material with controlled mesoporosity, achieved through the sol-gel reaction of tetraethyl orthosilicate (TEOS) at mild temperatures with the addition of different calcium concentrations. The resultant silica inks exhibited high printability and shape fidelity, while maintaining bioactivity and biocompatibility. Notably, the increased mesopore size enhanced the incorporation and release of large molecules, using cytochrome C as a drug model. Due to the varying surface charge of silica depending on the pH, a pH-dependent control release was obtained between pH 2.5 and 7.5, with maximum release in acidic conditions. Therefore, silica with controlled mesoporosity could be 3D printed, acting as a pH stimuli responsive platform with therapeutic potential.

1. Introduction

One of the recent milestone of bone tissue engineering has focused on the development of 3D printable materials to produce custom-made scaffolds with the desired defect shape and controlled macroporosity, which has an impact in the regeneration process [1,2]. To further enhance the regeneration process, bioactive molecules are incorporated within the scaffolds, allowing scaffolds to act as a drug delivery system and release drug at the defect site [3,4]. The scaffolds need to be designed with the appropriate intrinsic properties to allow the release of big sized molecules, such as proteins, and also have the capacity to release these molecules at specific conditions or time points.

Nowadays, the most commonly used materials for the 3D printing of scaffolds for bone regeneration are ceramics, mainly calcium phosphate or silica based. However, these materials usually require the use of high temperatures, which do not allow the encapsulation of molecules for the release [5]. Additionally, these high temperatures also decrease specific surface area of resultant materials, which could in turn limit the capacity to adsorb molecules [6–9]. Nevertheless, there are few selected number of materials that can be processed and 3D printed at mild temperatures. For instance, some 3D printable calcium phosphates have been developed, showing the capacity to encapsulate molecules within their structure. While in the case of calcium phosphates, albeit of their encapsulation capacity, their sustained release capacity of molecules is moderate which is mainly related to the overall pore size of calcium phosphates [10]. As an example of the low temperature calcium phosphate, cements are considered a very promising type of material for their use in rapid prototyping and their capacity to used them as ink has a direct relationship with the mechanical properties as well as with the intrinsic porosity of the structure. In this sense, it was determined that structures obtained with lower mechanical stability possess higher pore size in the sub-micron range which allowed proper drug delivery capacity, whereas higher resistance structures limit their use as drug delivery platforms due to their smaller sized pores. Hence, obtaining calcium phosphate based scaffolds that allow the proper 3D printing together with an appropriate drug eluting capacity will intrinsically depend on the pore size of the structure which will ultimately determine the mechanical properties of the substrate.

With this in mind, we have previously developed a printable silica based material produced at mild temperatures using tetraethyl orthosilicate (TEOS) sol-gel reaction [11]. Similar to calcium phosphates, silica-based inks lack of a large pore size and hence possess limited delivery of large molecules, such as growth factors. This jeopardizes the release of the cargo encapsulated within the structure and hence may

* Corresponding author. Bioengineering Institute of Technology (BIT), Universitat Internacional de Catalunya (UIC), Barcelona, 08017, Spain.
** Corresponding author. Bioengineering Institute of Technology (BIT), Universitat Internacional de Catalunya (UIC), Barcelona, 08017, Spain.
E-mail addresses: lmdelgado@uic.es (L.M. Delgado), rperezan@uic.es (R.A. Pérez).

https://doi.org/10.1016/j.mtbio.2024.101187
Received 20 June 2024; Received in revised form 31 July 2024; Accepted 5 August 2024
Available online 9 August 2024

limit the beneficial effect of the encapsulated molecules. However, these low temperature silica based materials have shown the capacity to release in a sustained manner the entrapped molecules found within its structure [12]. In order to overcome this problem, the incorporation of calcium to a similar sol-gel reaction was proposed to increase pore size of silica microspheres, providing sufficient space for the release of bigger sized biological molecules. Therefore, adding calcium to the pure silica ink could allow its use as a drug delivery system for large molecules [12]. While this solves the release of bigger sized molecules, there is still little control over the release of the molecules, despite the release was previously shown to be nearly zero order kinetics.

In this sense, in general, delivering the cargo incorporated in the scaffolds is essential to trigger the several processes the scaffolds have been designed for. However, it is known that initial burst release, which leads to high percentage of the cargo released within the initial hours and days, may limit triggering certain processes for which the scaffold has been designed. Taking into account for instance conditions in which bone can be under certain disease, infection or residual cancer, strategies to have specific release only under these conditions are essential. Situations such as residual tumor tissue or severe infection can lead to recurrence of the disease or sepsis, which need to be treated to reduce the potential life threats.

In this sense, taking into account the net charge of silica-based scaffolds and how their surface charge can be tuned by the environment, we considered the pH dependent release from silica-based scaffolds as a promising strategy to overcome abnormal bone conditions. Silica has been previously used as pH-dependent drug delivery system, taking advantage of silica surface charge variation at different pH and creating a smartly designed endogenous stimuli-responsive system [13]. Taking into account that silica has an isoelectric point between 2 and 5, and that it is negatively charged at physiological pH, while shifting to neutral at acid pH [14,15]. In this way, the incorporation of a molecule with a high isoelectric point, such as cytochrome C, would theoretically allow to control the release rates due to attraction and repulsion forces as the pH changes [16]. While cytochrome C may be used as a model molecule, other molecules with regeneration/antibacterial/anti-inflammatory capacity with similar morphologies and surfaces charges as cytochrome *c* can be used. Previous studies achieved pH-controlled release by inducing material degradation and, in turn, release of the encapsulated drug [17,18].

Therefore, the aim of this study was to obtain silica inks with higher pore sizes that could be used for the pH-dependent release of bioactive molecules. To do this, calcium was incorporated at different concentrations, expecting an increase in pore size without any negative effect on the cell behavior and bioactivity. Moreover, to analyze the pH-dependent release, cytochrome C was used; its adsorption on the surface was preferred opposed to encapsulation based on previous works in which the encapsulation presented a sustained and long-term release, while in this work we aim for a controlled short release.

2. Materials and methods

2.1. Ink preparation

Main reagents for the calcium-doped silica-based inks were tetraethyl orthosilicate (TEOS, Sigma-Aldrich), hydrochloric acid (HCl; 37 %, Honeywell) and calcium chloride ($CaCl_2{\cdot}2H_2O$, Sigma-Aldrich). The designed ink is based on the sol-gel transition of silica based material and its preparation was similar to a previous study [11]. Briefly, 10 mL TEOS was mixed with 4 mL of H_2O and 2.4 mL of HCl 0.1M, obtaining a molar ratio H_2O/TEOS of 8 (including the HCl). In the case of the calcium-doped inks, the right amount of $CaCl_2{\cdot}2H_2O$ was added to obtain a $CaCl_2$ molar ratio of 10, 20 and 30 % (0.72, 1.62 and 2.76 g respectively, for 10 mL of TEOS) [19], for which the amount of water was adjusted to maintain identical the H_2O/TEOS molar ratio. Based on their calcium content, the groups were categorized as follows: 0 % Ca, 10 % Ca, 20 % Ca, and 30 %. In order to incorporate de $CaCl_2$, the salt was dissolved in the H_2O + HCl mixture, prior to the sol preparation. The reagents were vigorously stirred at 700 rpm until the hydrolysis process was finalized and the sol was prepared. The pH of each sol was measured using a pH-meter (Seven Compact Duo pH/Conductivity pH meter, Mettler Toledo) in triplicates to observe the possible effect of calcium in the initial pH of the sol, which could in turn affect the gelling reaction.

To initiate the gelling reaction, sols were introduced in a water bath at 60 °C while stirring. Then, sols were placed in 3 mL syringes to continue the reaction before initiating the gelling process. In order to obtain a printable ink, the sols required an initial gelling. This initial gelling that allowed printability of the gel was considered reached once a gel could be printed when it could be extruded through a 0.58 mm nozzle without breaking and being able to stack up layers for at least 30 min. This initial time required until the sols were ready to be printed was measured.

2.2. Shape fidelity assessment

The shape fidelity of the different inks was assessed by using three different tests based on the work done by Ahasan Habib et al. [20]. The tests determine diffusion rate (D_{fr}), printability (P_r) and material collapse (C). For the D_{fr}, values around 100 % indicate severe ink diffusion, whereas the minimum value is 0 % that would mean there is a high shape fidelity. For the P_r, a value equal to 1 shows the printing of a perfect square, whereas lower values indicate morphology similar to a circle. Finally, high C values indicate a lower ability to bridge the gap at the measured distance. Based on image analysis of the different printing patterns (Supplementary Fig. 1), these values were calculated and allowed assessing how accurate the printing was.

2.3. 3D printing of scaffolds and contraction assessment

Inks were printed with a BioX 3D printer (Cellink), using a mechanical extrusion or direct ink writing system. The used parameters were 0.58 mm nozzle, 2.50 μL/s as an extrusion rate, 10 μL as a retract volume and 7 mm/s speed to 3D print 15x15 × 3 mm^3 scaffolds. Once the scaffolds were printed, they were placed in a container, closed with parafilm and aged for 2 days at 37 °C to finish the sol-gel reaction, and then dried at room temperature for at least 24 h.

Moreover, the contraction of the material after the drying step was also quantified. For this purpose, scaffolds were measured with a caliper just after 3D printing and after completing the drying process previously explained. All measures were done in triplicates.

2.4. Scanning electron microscopy

3D printed scaffolds were observed with a scanning electron microscopy (SEM) (JSM 5410, JEOL) at a voltage of 10 kV. For this purpose, samples were previously coated with a gold layer using a sputter coater (AGB7340, Agar Scientific). Energy dispersive X-ray spectroscopy (EDS) was used to analyze the chemical composition of sample surface.

2.5. Mesopore distribution and surface area

The mesopores and surface area of the material were analyzed by N_2 gas adsorption/desorption, using the Brunauer–Emmett–Teller (BET) method measured by using ASAP 2020 adsorption analyzer (Micromeritics). Scaffolds were 3D printed, crushed into small pieces and degassed for 10 h at 150 °C. The Barret-Joner-Halenda (BJH) method was used to estimate the pore size distribution and the total pore volume was calculated from the gas amount adsorbed at a maximum relative pressure (P/P0).

2.6. Compression test

Compression test of 10x10 × 10 mm^3 scaffolds was performed using a universal testing machine (Z5, Zwick). Scaffolds were hydrated overnight and measured with a caliper prior to the mechanical testing. All scaffolds were deformed to complete failure (deformation rate of 1 mm/min). The following parameters were assessed: maximum force (N), strain at break (%) and elastic modulus (MPa).

2.7. Cell toxicity and morphology assessment

To analyze the ability of cells to adhere and proliferate on the scaffolds, rat mesenchymal stem cells (rMSCs) were used. The cells were isolated from bone marrow of five-week-old male Sprague-Dawley rats. Briefly, rats were euthanized, collecting femur and tibia bones. Then, cells were harvested, passed through a 40 μm cell strainer and centrifuged at 1500 rpm for 3 min. Cells were maintained in Advanced DMEM (Gibco), containing 10 % of fetal bovine serum (FBS, Sigma), 1 % of Penicillin-Streptomycin (Gibco) and 1 % GlutaMAX solution (Gibco) in a humidified atmosphere with 5 % CO_2 in air. Cells were seeded on 175 cm^2 flasks and cultured until they were 80–90 % confluent. Then, they were treated with accutase (Gibco) to detach cells and used for the experiments.

Scaffolds were 3D-printed, aged, dried and sterilized through UV light for 30 min. Scaffolds were left overnight with complete media, after which the cells were seeded on top of the scaffolds. To avoid cell adhesion to the plate, all cell cultures were performed in 48-well plates covered with sterile agarose 1 % (Fisher). Cells were seeded with complete media at a density of 60.000 cells per scaffold. Moreover, cells were seeded on the TCP of 24-well plates as positive and negative controls. After 2.5 h, culture media was removed and 300 μL of fresh media were added to remove non-adhered cells.

To determine the potential cytotoxicity of the scaffolds, an LDH assay was performed following the manufacturer protocol (CyQUANT, Invitrogen). Briefly, media was recovered from the wells, which were replenished with 300 μL of fresh media, storing the samples afterwards at −80 °C after 1, 3 and 7 days of culture. As negative control, cells cultured in TCP were lysated with 10 μL of Lysis Buffer and incubated at 37 °C for 45 min. Then, controls and thawed samples were mixed with LDH Reaction Mixture at a ratio 1:1 and incubated at room temperature for 30 min. Then, absorbance of each sample was measured at 490 and 680 nm, using a plate reader (Infinite M Nano, TECAN). The % of cytotoxicity was estimated for each condition.

Additionally, an immunofluorescence staining was performed to observe cell morphology and colonization of scaffolds. Cells were seeded as previously explained and, after 7 days of incubation, scaffolds were washed with 1x PBS and fixed with 4 % PFA for 40 min. Subsequently, scaffolds were washed twice with PBS and stained with Acti-Stain 488 phalloidin (Cytoskeleton, Inc) by diluting 7 μL phalloidin per mL of PBS and incubating the scaffolds with 500 μL of the solution for 45 min. Then, scaffolds were washed thrice with PBS to remove the excess of phalloidin. DAPI ready-made solution (Sigma-Aldrich) was used to stain the cell nuclei by diluting it 1:1000 in PBS and incubating for 30 s. Finally, the scaffolds were washed with PBS, and were observed in the confocal microscope (DMi8, Leica) using Alexa 488 and DAPI filters.

2.8. Bioactivity

Scaffolds were 3D printed aged, dried and washed with distilled water thrice. Simulated body fluid (SBF) was prepared following a previous formulation, containing the necessary ions for apatite deposition [21]. Scaffolds were sterilized by using UV-light for 30 min and incubated in water for 24 h. Then, scaffolds were immersed in 15 mL of SBF each, and incubated for 7 and 14 days. After each specified period, scaffolds were removed from the SBF solution and gently washed with H_2O three times, followed by a final drying process in a vacuum chamber. The deposition of apatite on the surface of the scaffolds was observed with the help of a scanning electron microscopy as explained in section 2.4.

2.9. Cytochrome C adsorption rate

To prove the ability of scaffolds to release molecules, cytochrome C (cyt C, Sigma-Aldrich) was adsorbed on the surface of the 0 % and 30 % scaffolds. As mentioned in the introduction, the molecule was adsorbed on the surface as opposed to encapsulating the molecule to obtain a fast release. This model protein was used as it has similar molecular size and charge compared to many growth factors. For the adsorption, scaffolds were 3D printed and dried, and they were immersed in a solution with 500 μL of cyt C in distilled water at a concentration of 500 μg/mL. After 1, 3, 7, 10 and 14 days, the cyt C solution in which scaffolds were immersed was used to estimate the adsorption rate by measuring the absorbance at 408 nm, and extrapolating the adsorbed concentration using a standard curve ranging from 10 to 500 μg/mL.

2.10. Cytochrome C pH-dependent release

Cytochrome C release was studied at different pH; nine different pH were used: pH 2, 2.5, 3, 3.5, 4, 4.5, 5, 5.5 and 7.5. The pH solutions were prepared by using a citric acid-sodium citrate buffer, mixing the right proportions to obtain the desired pH. Then, cyt C loaded scaffolds were immersed in 500 μL solutions of those pH and kept at 37 °C. At different time points, 1, 3, 7, 14, 21 and 30 days, the solutions were retrieved and measured at 408 nm to estimate the release. The release was measured by checking the absorbance at 408 nm and extrapolating the released concentration by using a standard curve ranging from 10 to 200 μg/mL.

Moreover, the ability to control the release using different pH was quantified to assess the effect of pH in the release rate. For this purpose, two different pHs were used, mainly 2.5 and 5.5, which combined a rather acidic pH with a rather neutral pH. The cyt C loaded scaffolds were immersed in a solution with a pH of 5.5 for 24 h, after which the release was measured, and the scaffold was moved to a pH 2.5 solution for another 24 h. This was repeated up to day 8 days.

2.11. Statistical analysis

Statistical analysis was performed using MiniTab 17 software (Minitab Inc.). One-Way ANOVA parametric test and Kruskal-Wallis, and Mann Whitney U non-parametric tests were used to compare the different conditions to each other. Statistical differences were considered with $p < 0.05$.

3. Results and discussion

3.1. Ink preparation

Calcium was incorporated at three different concentrations within TEOS sol to increase pore size of the material. As ions can alter sol-gel reaction kinetics, the time to form a sol, initial pH and gelling time was measured (Fig. 1).

The time to form a sol for each calcium concentration is represented in Fig. 1a. Higher concentrations of calcium increased the duration of the hydrolysis process. This can be related to the ion crowding, due to the size and also positive charge which can produce stearic repulsion, making it more complicated for the TEOS and water molecules to interact [22]. Moreover, the initial pH of the sol was different in each case, as seen in Fig. 1b. In this case, as the amount of calcium increased, the pH decreased, being as low as 0.9 for concentrations of 30 %. This can be explained based on the ability of calcium to incorporate the hydroxide group of H_2O, forming $Ca(OH)_2$, therefore releasing a proton which in turn acidifies the sol.

All sols were gelled at 60 °C as in a previous work, showing that this

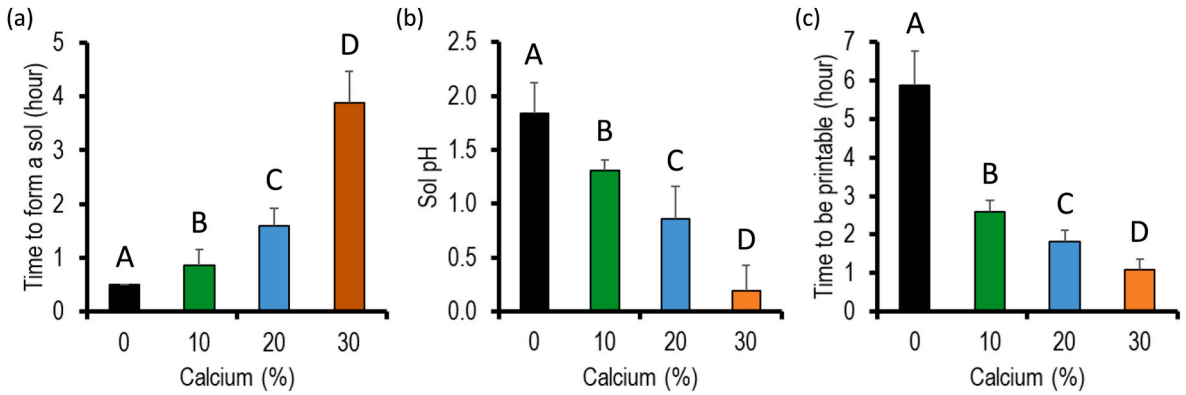

Fig. 1. (a) Time in hours to form a sol, (b) initial pH of the formed sols for each of the calcium concentrations and (c) time to reach a printable stage at 60 °C for each of the calcium concentrations. Statistically significant differences were found between groups A, B, C and D ($p < 0.05$).

temperature reduces printing time without introducing defects of the 3D printed struts [11]. The time needed for the inks to be ready for printing were estimated in triplicates. Fig. 1c shows the required time for each sol to achieve sufficient viscosity to be considered printable. The concentration of calcium played an important role, showing that the 30 % condition became printable after 70 min, presenting a significantly shorter time compared to the nearly 6 h needed for the 0 % concentration. This indicates that the presence of higher calcium concentrations in the inks expedite the gelling time of silica. This fact may be related to the isoelectric point of silica, which is approximately found at pH 2, which matched that of the 0 % sol. With the introduction of calcium, which lowered the pH, the disparity between sol pH and the silica isoelectric point increased and this larger gap likely triggered the gelling reaction, accelerating the process and reducing the overall reaction time. Interestingly, this reduction in the time to be printable is a notable feature for potential translation. Additionally, the gelling reaction can be partially halted by storing the material at −20 °C for several weeks [23]. Furthermore, this reaction takes place at mild temperatures and pH, when other bioceramics require high temperature steps with higher environmental impact [24]. In turn, mesoporosity is preserved, allowing for the encapsulation of higher drug amounts [25,26].

3.2. Shape fidelity and contraction assessment

Shape fidelity was evaluated by measuring diffusion rate, printability and material collapse. These parameters define the proximity of the 3D

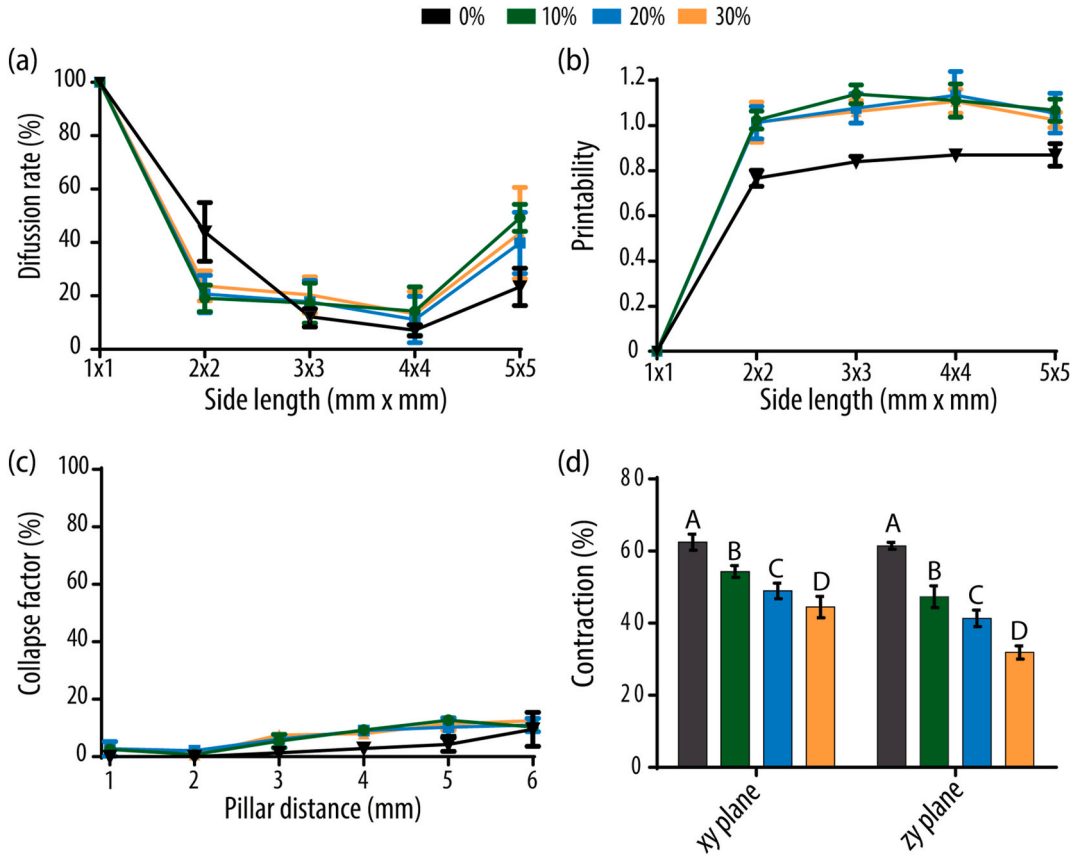

Fig. 2. Shape fidelity assessment including (a) diffusion rate, (b) printability, (c) collapse factor of each of the inks and (d) contraction of the different 3D-printed scaffolds after drying at room temperature for 3 days. Statistically significant differences were found between groups A, B, C and D ($p < 0.05$).

printed scaffold to the intended shape, while establishing the minimum pore sizes and filament distances crucial for achieving high printing accuracy. Anticipating these factors enables the precise design of the scaffold to meet specific requirements and to obtain a custom-made scaffold with a specific shape, size and pore geometry, which are proven to affect the tissue regeneration process [27,28].

Regarding diffusion rate (D_{fr}, Fig. 2a), calcium-incorporated inks showed 100 % diffusion for the smallest pore, as it could not be properly printed. This fact was also observed for the pristine silica inks. It is worth pointing out that the D_{fr} decreased as the pore size increased, except for the biggest pore, which was affected by a rounding effect at the corners. Moreover, there were differences between the pristine silica and the calcium-doped inks for the same pore sizes. In the case of 2 × 2 mm^2 pore, the addition of calcium decreased the D_{fr}, being able to print smaller pores with a higher accuracy than the pristine silica. However, in the case of the corner pore, 5 × 5 mm^2, the D_{fr} was lower for the pristine silica, meaning the rounding of the corner is higher for the calcium containing inks. These results highlight the ability of the calcium-incorporated inks to accurately print pores of a minimum size of 2 × 2mm^2, being an improvement when comparing to the pristine silica, which only allowed proper printing from 3 × 3mm^2, while being negatively affected on the printing of the corner pore, which is important to keep in mind when designing the scaffold and designing a 3D printed scaffolds [29].

Regarding the printability (P_r, Fig. 2b), the pristine silica showed a value close to 0.8 for all the side lengths, which meant they had a rounded shape. The addition of calcium caused a significant difference, the P_r being higher than 1 in all cases, between 1 and 1.1, meaning that the pores geometry were still very close to the model, but instead of a rounding of the pores, there was a zig zag printing. In all cases, the square geometry was still close enough to the model to be considered an adequate shape fidelity.

Finally, calcium-incorporated inks behaved in a similar fashion to the pristine silica in terms of material collapse (C, Fig. 2c), increasing as the gap lengths were bigger. In general, the C was higher in this case, but still being lower than 15 % in all cases, therefore the inks successfully bridged the gap in distances up to 6 mm, without having a significant collapse.

Another element that is important to consider when designing scaffold is the post-drying contraction. This includes assessing both the contraction percentage, to estimate the final scaffold size, and ensuring uniform contraction across all dimensions. All conditions showed a homogenous contraction, with no significant deformations. The pristine silica showed a very high contraction, above 60 % in both planes, whereas the addition of calcium lowered the contraction, as seen in Fig. 2d. The results showed that as the calcium percentage increased, there was a lower contraction, reaching as low as 42 % in the xy plane and 30 % in the zy plane for the 30 % condition. The contraction in the zy plane is related to the lateral porosity, therefore it is positive that this contraction is lower than in the xy plane, reducing the potential lateral pore loss due to the contraction. The decrease in contraction with the incorporation of calcium can be explained due to larger mesopore size and a change in the reaction speed, increasing condensation ratio while retaining higher amount of water and ultimately decreasing the contraction [30].

3.3. Scaffold morphology

SEM microscopy revealed that scaffolds retained their structural morphology and open pores despite large contractions (Fig. 3a). The resultant patterns were straight and well-defined, superior to other standard materials [31]. The struts appeared uniformly rounded and well-defined across all conditions. Additionally, EDS analysis confirmed the predominant presence of silicon in the scaffolds, validating the pure silica composition. Notably, the gold detected originated from the conductive coating applied prior to the SEM analysis.

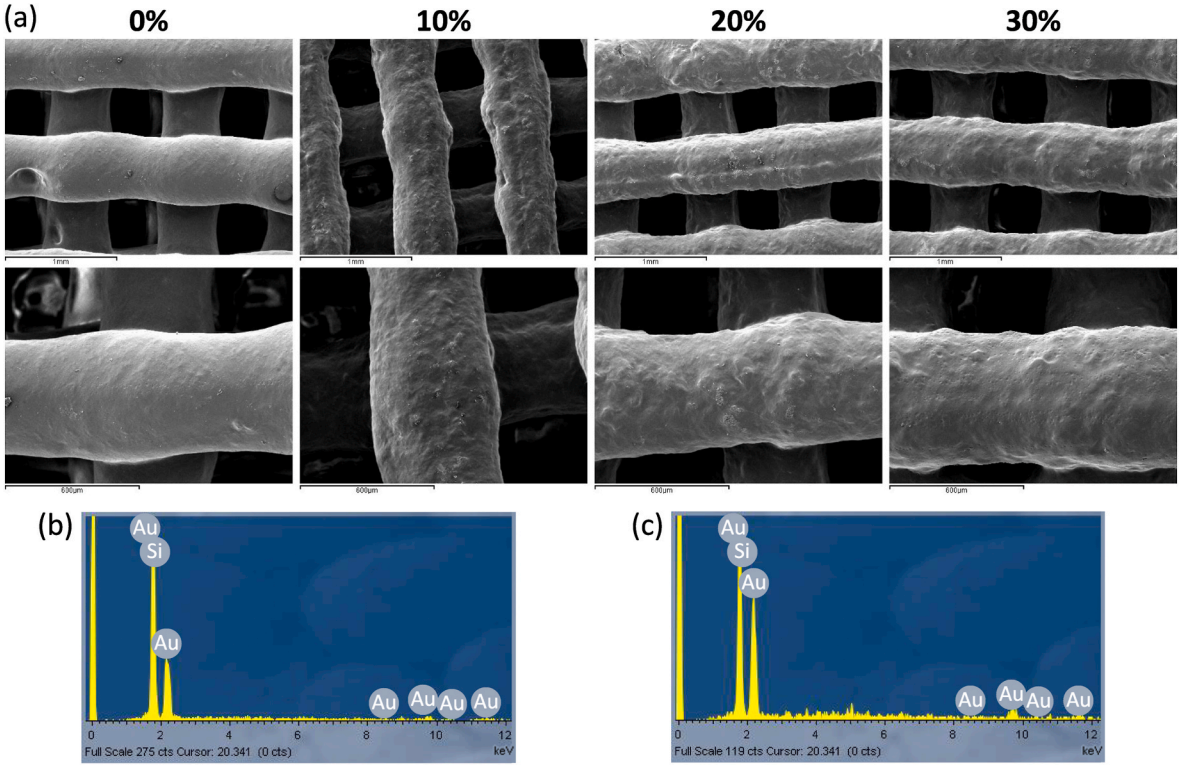

Fig. 3. Scanning electron microscopy (SEM) analysis. (a) SEM images of scaffold structure and strut with the different calcium concentrations. EDS analysis at 0 % (b) and 30 % (c) after washing, demonstrating that scaffolds are mainly composed of silicon.)

3.4. Mesopore distribution and surface area

Porosity and surface area are important features of the sol-gel silica-based materials, which have an effect on drug loading and release capacity of the material as well as cell response and even osteogenic differentiation [32].

Fig. 4a showed the N_2 adsorption/desorption isotherms which determined the mesoporosity of the material. For the 0 % and 10 %, the isotherms showed hysteresis loops, precisely a type I, whereas the two with the higher amount of calcium, 20 % and 30 % showed a type IV isotherm. A type I isotherm indicates that the material is a microporous solid with a pore size <2 nm, and a type IV means the presence of mesoporosity within the material, with pore size as >2 nm and <50 nm [33]. This is confirmed with the data of the pore sizes and specific areas, which can be seen in Fig. 4a, concluding that the proportion of calcium had a direct impact in the pore size distribution, going from a pore size of 1.66 nm for 0 %, up to 8.10 nm for the highest concentration. As seen in Fig. 4a, the incorporation of calcium also increased the pore volume, from 0.24 cm^3/g in the case of 0 %–0.47 cm^3/g for the highest calcium concentration. Moreover, the surface area behaved in the opposite way, decreasing with increasing calcium, going from 569.51 m^2/g to as low as 232.53 m^3/g. Therefore, the calcium addition increased the number of pores as well as the size of the pores, although showed a decrease of the total surface area of the material, which was already observed in our previous studies where calcium was incorporated to the silica sol-gel reaction [34]. This can be again explained with the size of the incorporated ion, similarly to the sol-gel reaction speed, as the presence of calcium ions redistributes the silica interconnected network, creating less but bigger pores.

Indeed, the small pore size of pure silica limit the drug release capacity to small molecules such as ibuprofen with a slow release rate [35–37]. As the pore size increased for the 20 % and 30 % conditions, it enables the incorporation of larger molecules, such as growth factors, which are known for having a highly positive effect on the osteogenecitiy of the material [38]. This bigger pore size also would allow the encapsulation of small molecules, but in this case, the release would be faster than in the pure silica. Therefore, depending on the desired biomolecules to deliver, different proportions of calcium should be used to obtain the adequate porosity [39].

3.5. Mechanical properties

Compression test assays demonstrated a typical brittle behavior with low deformation, being less than 6 %, and a maximum force, lower than 120N (Fig. 4b). All calcium doped silica inks showed a saw-like behavior related to minor strut breaks before the total failure. This fragile behavior was described previously for pure silica forms [11,40]; however, these mechanical features may be sufficient compared with other 3D printed bioceramics [41]. Although there was no significant statistical difference ($p > 0.05$), all calcium doped silica inks demonstrated a tendency to lower deformation capacity when compared to pristine silica.

3.6. Cytotoxicity and adhesion

The results of the cytotoxicity assay are represented in Fig. 5a. Any cell death below 20 % compared to the control would mean the material is not cytotoxic, whereas cell death between 20 and 40 % indicates moderate cytotoxicity [42].

The positive control showing the spontaneous LDH activity on TCP was below 20 % with the exception of day 7, that showed a 25 % cell death, which can be related with the excessive confluence of the cells in the well after 7 days.

In the case of the silica-based scaffolds, for all time points the cell death did not raise above 20 %, proving the lack of cytotoxicity of the material, as expected from previous studies using the same proportion of calcium, which did not observe any negative effect on the cell growth [34]. Moreover, no significant differences were found between the pristine silica and the calcium-doped conditions.

Moreover, the immunofluorescence images shown in Fig. 5b

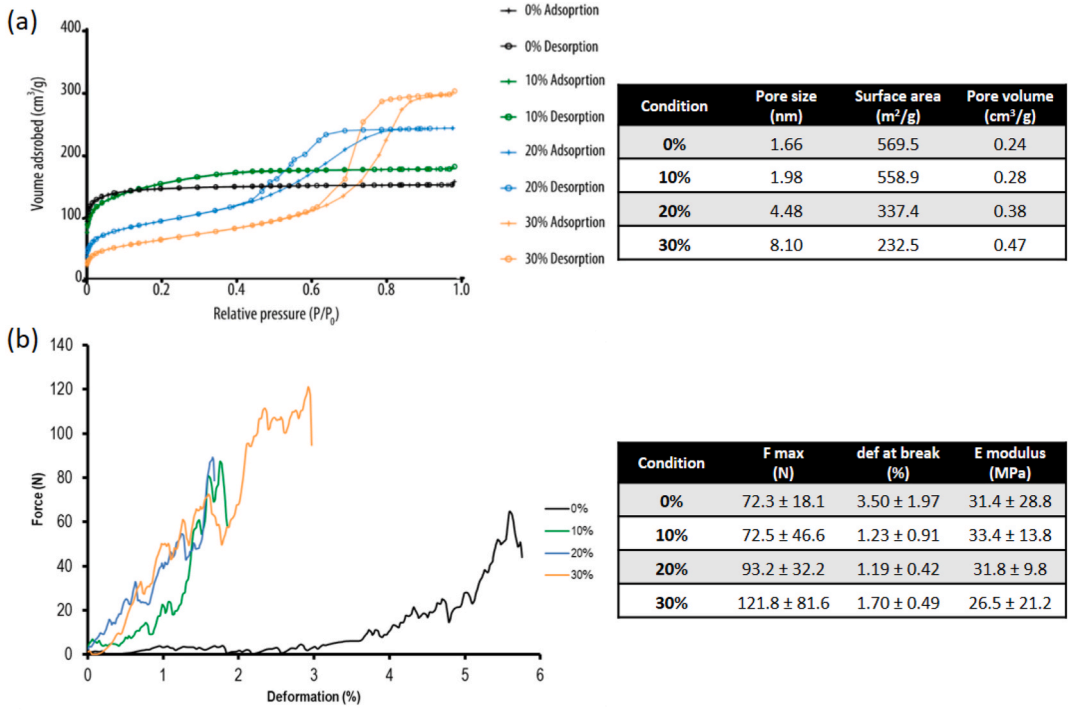

Condition	Pore size (nm)	Surface area (m^2/g)	Pore volume (cm^3/g)
0%	1.66	569.5	0.24
10%	1.98	558.9	0.28
20%	4.48	337.4	0.38
30%	8.10	232.5	0.47

Condition	F max (N)	def at break (%)	E modulus (MPa)
0%	72.3 ± 18.1	3.50 ± 1.97	31.4 ± 28.8
10%	72.5 ± 46.6	1.23 ± 0.91	33.4 ± 13.8
20%	93.2 ± 32.2	1.19 ± 0.42	31.8 ± 9.8
30%	121.8 ± 81.6	1.70 ± 0.49	26.5 ± 21.2

Fig. 4. (a) N_2 adsorption/desorption isotherms measured by the BET method of the pristine silica and calcium-doped printed scaffolds. Summary of the pore size, surface area and pore volume obtained by the BET method. (b) Mechanical testing: representative compression test – stress strain curve for each calcium concentration. Summary of maximum force (N), deformation at break (%) and elastic modulus (E).

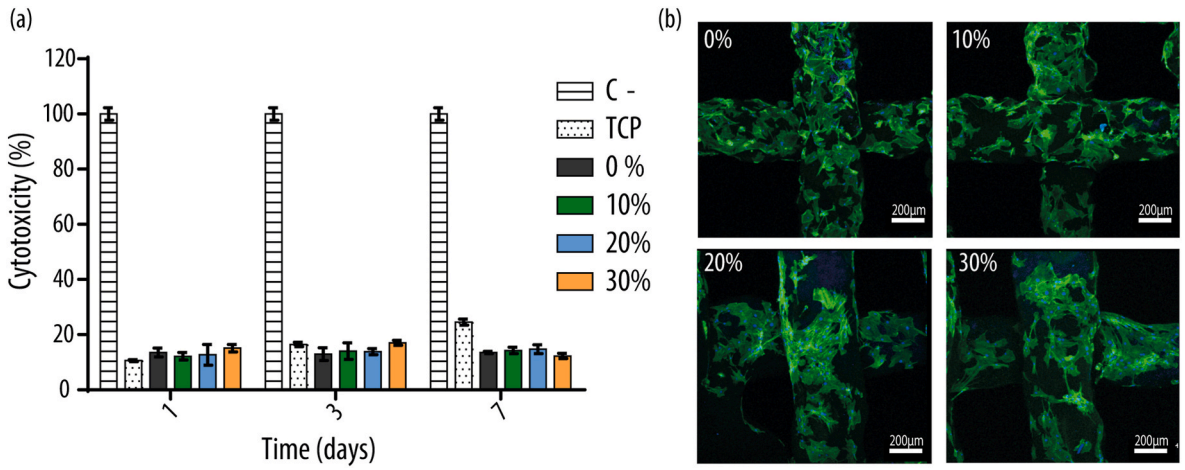

Fig. 5. In vitro cell culture. (a) Cytotoxicity estimated by doing a LDH assay after 1, 3 and 7 days and (b) Immunofluorescence images for DAPI (blue) and phalloidin (green) after 7 days of cell culture on the different conditions. No significant differences were found in the calcium-doped inks when comparing to pure silica.

demonstrated a similar cell morphology in all cases, with elongated cells meaning they were properly attached to the scaffold. The cell distribution was equal in the 0 % and 10 % scaffolds, with the cells spread and separated; whereas in the case of the higher calcium concentrations, 20 % and 30 %, the cells formed some agglomerates on the struts.

3.7. Bioactivity

The bioactivity was analyzed on the two extreme conditions, 0 % and 30 %, and those that showed larger difference on the pore size. Both conditions promoted apatite-like crystals formation at approximately

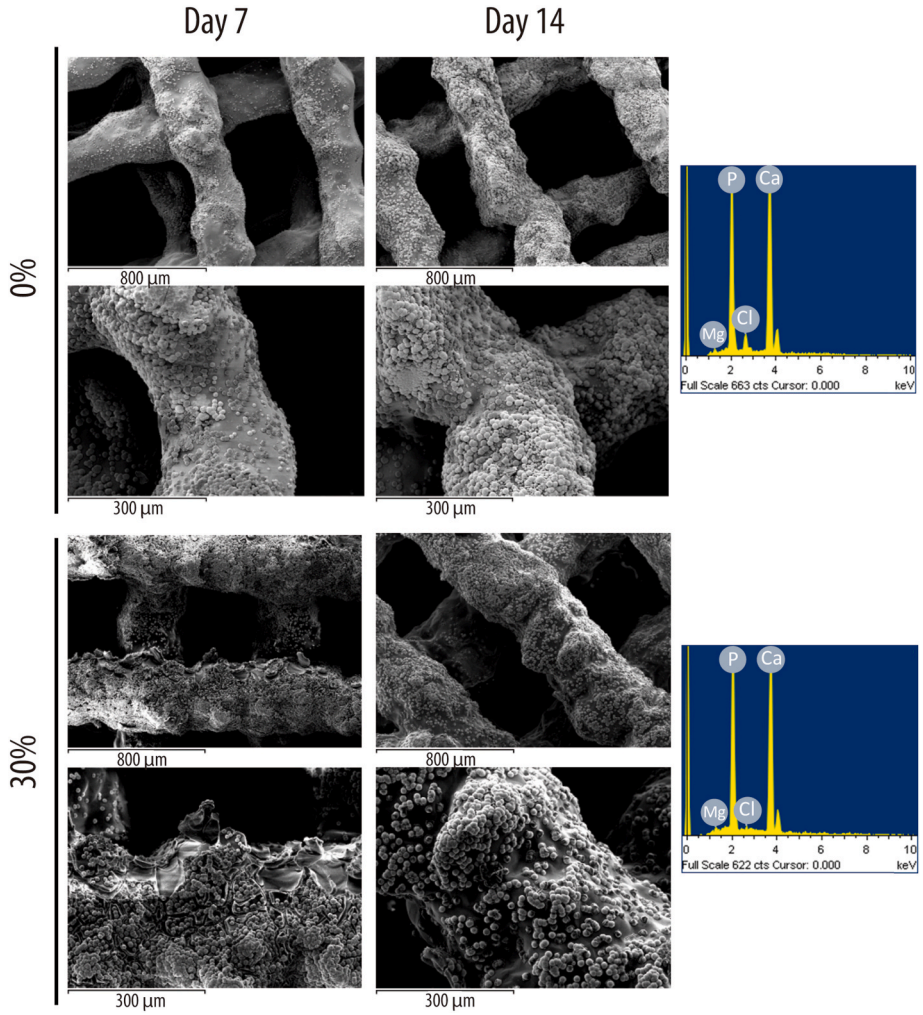

Fig. 6. SEM images of the 0 % and 30 % 3D printed scaffolds after 7 and 14 days incubated in SBF at 37 °C to observe the apatite formation. EDS analysis of precipitates at day 7 confirmed the presence of calcium and phosphate ions.

the same time, showing a clear mineral deposit after 7 days of incubation in SBF, as seen in Fig. 6. Moreover, EDS was performed on the ceramic crystals formed, confirming the presence of calcium and phosphate ions. The negative control did not show any sign of apatite-like precipitate patterns (Supplementary Fig. 2). Although a previous publication on calcium-doped silica microspheres showed a similar deposition time [34], the apatite-like crystals observed on both scaffolds were larger at day 7. This difference could be explained due to the roughness and irregularity of the surface of 3D printed scaffolds, compared to the smoothness of a microsphere. Overall, the addition of calcium to sol-gel silica-based inks did not show any change in the bioactivity.

3.8. Cytochrome C adsorption

Cytochrome C was incubated with 30 %, as it was the condition with the higher pore size, and, therefore, the one in which this type of molecule could easily be adsorbed for its release. The adsorption profile can be seen in Fig. 7a showing that after 5 days, the adsorption reaches a plateau, meaning that it cannot absorb any more cytochrome C within the scaffold structure, making up an 84 % of the protein adsorbed. 0 % was used as control, showing no cytochrome C absorption at all.

3.9. Cytochrome C pH-dependent release

The cytochrome C loaded scaffolds were incubated with buffers at different acidic pH, from 2.5 to 7.5, to see the effect of pH on the release rates. The release results at each pH can be seen in Fig. 7b, showing larger cytochrome C release as pH was lower, and that there was no detectable cytochrome C release at pH 7.5. When the pH was 5.5 or lower, there was an initial burst release in the initial 24 h, followed by a fast cytochrome C release up to 72 h. After that, the release rate decreased to almost zero kinetics, continuing the release up to 28 days in all cases except for pH 5.5, which ceased the release after 21 days. In all cases, the release pattern is similar, with a difference in the total amount of cytochrome C that was released, being much higher for lower pH.

The reason behind the differences in released cytochrome C can be explained referring to the silica surface charge at different pH. Cytochrome C is a highly positively charged molecule, with an isoelectric point of near 10 [43,44], while silica is negatively charged at pH above −5 when present in a flat surface, which can also be affected by the silica size and shape [44,45]. This explains the lack of release at physiological pH, as cytochrome C is positively charged and silica very negatively charged; therefore, the electrostatic interaction does not allow the molecule to be released from scaffolds. Regarding the rest of the pH, as the pH decreased, the negative charge of the silica scaffold was decreasing, while the positivity of the cytochrome C was increasing, producing a faster and higher release of the molecule due to electrostatic repulsion. This could be very useful for a controlled release by a pH shift, obtaining a desired release using pH as an external controlling factor. Although previous studies achieved 3D printed scaffolds with pH stimuli responsive drug release [46,47], they did not demonstrate large difference between pH levels or the capacity to stop the release at a specific pH.

This pH control release was further proved by carrying out a cytochrome C release using two different pH, 2.5 and 5.5, showing that the release could be controlled by the pH of the surroundings, as seen in Fig. 7c. The starting pH was 5.5, obtaining an initial low release after 24 h. The following 24 h, the incubation media was changed to a pH of 2.5, obtaining a much higher and faster release. This was done up to 8 days, confirming that the release rate can be controlled with the pH, being able to change the molecule release to match the desired one.

This could prove beneficial, as pH levels tend to decrease during certain phases of bone regeneration or infections [13,48]. This drop in pH would promote the release of the adsorbed molecules, which would continue its release until reaching physiological levels. Moreover, the differences in release rates at acid pH would also allow having a faster release in cases where the drop in pH is high, caused by a more severe bone damage, being able to deliver a higher amount of the molecule to help the process. This controlled release makes the material very promising for drug delivery in bone regeneration process. Finally, our

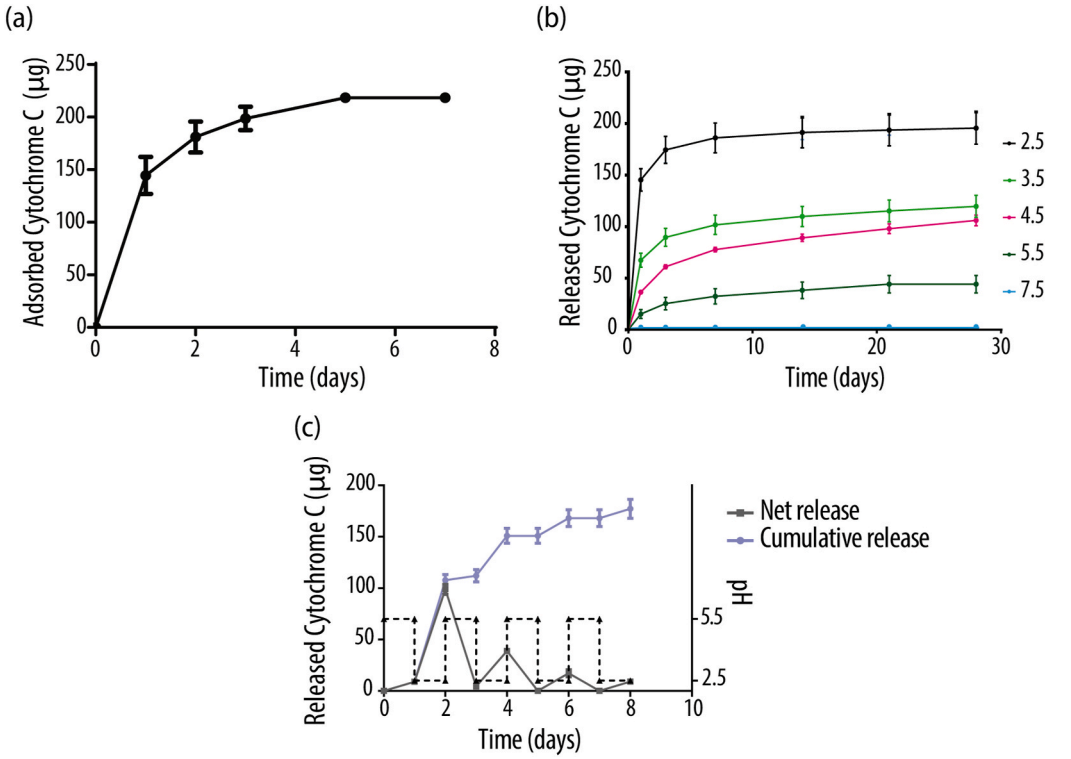

Fig. 7. (a) Cytochrome C adsorption up to 7 days of the 30 % scaffolds, (b) cumulative cytochrome C release at different pH ranging from 2.5 to 7.5 up to 28 days and (c) cytochrome C controlled release by alternating pH between 5.5 and 2.5 up to 8 days showed as net and cumulative release.

approach focused on large molecules and only 30 % calcium allowed their encapsulation. It is noteworthy that this platform could be adjusted for the release of small molecules with anti-inflammatory or anticancer potential, which can have a crucial function *in situ* after implantation [49,50]. In this sense, the condition with 10 and 20 % calcium could induce a pore size sufficient to absorb and retain small molecules for biomedical applications.

4. Conclusions

Calcium ion can be incorporated within pure silica inks prepared at mild conditions at different concentrations, up to at least 30 % of calcium, without losing the printing capacity. The incorporation of calcium lengthens the hydrolysis step, lowers the pH of the sol and shortens the condensation step, without having a significant negative effect on the printability and shape fidelity of the inks. Moreover, the presence of calcium did not alter the bioactivity of the material and did not cause any cytotoxicity in the material. Additionally, the incorporation of calcium allowed controlling the pore size, which was bigger for higher calcium concentrations. The increase of pore size allowed the adsorption of large molecules, such as cytochrome C. Furthermore, the release rate of this molecule can be controlled through pH, being faster for lower pH, which can be explained by surface charge of both silica and adsorbed molecule. Therefore, calcium-doped silica inks can be used as drug delivery systems and scaffolds for bone tissue engineering, being able to obtain a stimuli-dependent controlled release, which can enhance bone regeneration process.

CRediT authorship contribution statement

Raquel Rodríguez-González: Writing – original draft, Visualization, Validation, Methodology, Investigation, Formal analysis, Data curation. **José Ángel Delgado:** Writing – review & editing, Methodology, Investigation. **Luis M. Delgado:** Writing – review & editing, Writing – original draft, Visualization, Validation, Supervision, Project administration, Methodology, Investigation, Funding acquisition, Formal analysis, Data curation, Conceptualization. **Román A. Pérez:** Writing – review & editing, Supervision, Project administration, Investigation, Funding acquisition, Formal analysis, Data curation, Conceptualization.

Declaration of competing interest

The authors declare that they have no known competing financial interests or personal relationships that could have appeared to influence the work reported in this paper.

Data availability

Data will be made available on request.

Acknowledgements

This work was supported by the Government of Catalonia (2021 SGR 00565); the Spanish Ministry (Ramón y Cajal fellowship (RYC2018-025977-I), project PID2022-137962OB-I00 (MINECO/FEDER); and a predoctoral fellowship from Universitat Internacional de Catalunya (UIC).

Appendix A. Supplementary data

Supplementary data to this article can be found online at https://doi.org/10.1016/j.mtbio.2024.101187.

References

[1] H. Ma, C. Feng, J. Chang, C. Wu, 3D-printed bioceramic scaffolds: from bone tissue engineering to tumor therapy, Acta Biomater. 79 (2018) 37–59, https://doi.org/10.1016/j.actbio.2018.08.026.
[2] S. Bose, S. Vahabzadeh, A. Bandyopadhyay, Bone tissue engineering using 3D printing, Mater. Today 16 (2013) 496–504, https://doi.org/10.1016/j.mattod.2013.11.017.
[3] T. Limongi, F. Susa, M. Allione, E. Di Fabrizio, Drug delivery applications of three-dimensional printed (3DP) mesoporous scaffolds, Pharmaceutics 12 (2020) 1–18, https://doi.org/10.3390/pharmaceutics12090851.
[4] T.N. Vo, F.K. Kasper, A.G. Mikos, Strategies for controlled delivery of growth factors and cells for bone regeneration, Adv. Drug Deliv. Rev. 64 (2012) 1292–1309, https://doi.org/10.1016/j.addr.2012.01.016.
[5] C. Xin, Z. Li, L. Hao, Y. Li, A comprehensive review on additive manufacturing of glass: recent progress and future outlook, Mater. Des. 227 (2023) 111736, https://doi.org/10.1016/j.matdes.2023.111736.
[6] H. Zeng, J.L. Pathak, Y. Shi, J. Ran, L. Liang, Q. Yan, T. Wu, Q. Fan, M. Li, Y. Bai, Indirect selective laser sintering-printed microporous biphasic calcium phosphate scaffold promotes endogenous bone regeneration via activation of ERK1/2 signaling, Biofabrication 12 (2020) 025032, https://doi.org/10.1088/1758-5090/ab78ed.
[7] K.C.R. Kolan, M.C. Leu, G.E. Hilmas, M. Velez, Effect of material, process parameters, and simulated body fluids on mechanical properties of 13-93 bioactive glass porous constructs made by selective laser sintering, J. Mech. Behav. Biomed. Mater. 13 (2012) 14–24, https://doi.org/10.1016/j.jmbbm.2012.04.001.
[8] Y. Liu, T. Li, H. Ma, D. Zhai, C. Deng, J. Wang, S. Zhuo, J. Chang, C. Wu, 3D-printed scaffolds with bioactive elements-induced photothermal effect for bone tumor therapy, Acta Biomater. 73 (2018) 531–546, https://doi.org/10.1016/j.actbio.2018.04.014.
[9] H. Ma, C. Feng, J. Chang, C. Wu, 3D-printed bioceramic scaffolds: from bone tissue engineering to tumor therapy, Acta Biomater. 79 (2018) 37–59, https://doi.org/10.1016/j.actbio.2018.08.026.
[10] R. Trombetta, J.A. Inzana, E.M. Schwarz, S.L. Kates, H.A. Awad, 3D printing of calcium phosphate ceramics for bone tissue engineering and drug delivery, Ann. Biomed. Eng. 45 (2017) 23–44, https://doi.org/10.1007/s10439-016-1678-3.
[11] R. Rodríguez-González, L.M. Delgado, R.A. Pérez, Developing a pure silica ink for 3D printing through sol-gel reaction and mild conditions, J. Sol. Gel Sci. Technol. (2023), https://doi.org/10.1007/s10971-023-06228-1. Accepted.
[12] R.A. Perez, A. El-Fiqi, J.-H. Park, T.-H. Kim, J.-H. Kim, H.-W. Kim, Therapeutic bioactive microcarriers: Co-delivery of growth factors and stem cells for bone tissue engineering, Acta Biomater. 10 (2014), https://doi.org/10.1016/j.actbio.2013.09.042.
[13] M. Cicuéndez, J.C. Doadrio, A. Hernández, M.T. Portolés, I. Izquierdo-Barba, M. Vallet-Regí, Multifunctional pH sensitive 3D scaffolds for treatment and prevention of bone infection, Acta Biomater. 65 (2018) 450–461, https://doi.org/10.1016/j.actbio.2017.11.009.
[14] A. Gamero-Quijano, F. Huerta, E. Morallón, F. Montilla, Modulation of the silica sol-gel composition for the promotion of direct electron transfer to encapsulated cytochrome c, Langmuir 30 (2014) 10531–10538, https://doi.org/10.1021/la5023517.
[15] M. Barisik, S. Atalay, A. Beskok, S. Qian, Size dependent surface charge properties of silica nanoparticles, J. Phys. Chem. C 118 (2014) 1836–1842, https://doi.org/10.1021/jp410536n.
[16] S.H. Hristova, A.M. Zhivkov, Isoelectric point of free and adsorbed cytochrome c determined by various methods, Colloids Surf. B Biointerfaces 174 (2019) 87–94, https://doi.org/10.1016/j.colsurfb.2018.10.080.
[17] M. Asadi, Z. Salehi, M. Akrami, M. Hosseinpour, S. Jockenhövel, S. Ghazanfari, 3D printed pH-responsive tablets containing N-acetylglucosamine-loaded methylcellulose hydrogel for colon drug delivery applications, Int J Pharm 645 (2023) 123366, https://doi.org/10.1016/j.ijpharm.2023.123366.
[18] T. Huang, Z. Sun, D.E. Heath, N. O'Brien-Simpson, A.J. O'Connor, 3D printed and smart alginate wound dressings with pH-responsive drug and nanoparticle release, Chem. Eng. J. 492 (2024) 152117, https://doi.org/10.1016/j.cej.2024.152117.
[19] R.A. Perez, A. El-Fiqi, J.-H. Park, T.-H. Kim, J.-H. Kim, H.-W. Kim, Therapeutic bioactive microcarriers: Co-delivery of growth factors and stem cells for bone tissue engineering, Acta Biomater. 10 (2014) 520–530, https://doi.org/10.1016/j.actbio.2013.09.042.
[20] A. Habib, V. Sathish, S. Mallik, B. Khoda, 3D printability of alginate-carboxymethyl cellulose hydrogel, Materials 11 (2018) 454, https://doi.org/10.3390/ma11030454.
[21] T. Kokubo, H. Takadama, How useful is SBF in predicting in vivo bone bioactivity? Biomaterials 27 (2006) 2907–2915, https://doi.org/10.1016/j.biomaterials.2006.01.017.
[22] A. Vioux, L. Viau, S. Volland, J. Le Bideau, Use of ionic liquids in sol-gel; ionogels and applications, Compt. Rendus Chem. 13 (2010) 242–255, https://doi.org/10.1016/j.crci.2009.07.002.
[23] R. Rodríguez-González, L.M. Delgado, R.A. Pérez, Developing a pure silica ink for 3D printing through sol-gel reaction and mild conditions, J. Sol. Gel Sci. Technol. (2023), https://doi.org/10.1007/s10971-023-06228-1.
[24] K. Lin, R. Sheikh, S. Romanazzo, I. Roohani, 3D printing of bioceramic scaffolds—barriers to the clinical translation: from promise to reality, and future perspectives, Materials 12 (2019) 2660, https://doi.org/10.3390/ma12172660.
[25] S. Eqtesadi, A. Motealleh, R. Wendelbo, A.L. Ortiz, P. Miranda, Reinforcement with reduced graphene oxide of bioactive glass scaffolds fabricated by robocasting,

J. Eur. Ceram. Soc. 37 (2017) 3695–3704, https://doi.org/10.1016/j.jeurceramsoc.2016.12.047.
[26] R. Bento, A. Gaddam, P. Oskoei, H. Oliveira, J.M.F. Ferreira, 3D printing of macro porous sol-gel derived bioactive glass scaffolds and assessment of biological response, Materials 14 (2021) 5946, https://doi.org/10.3390/ma14205946.
[27] M.J. Jahir-Hussain, N.A. Maaruf, N.E.F. Esa, N. Jusoh, The effect of pore geometry on the mechanical properties of 3D-printed bone scaffold due to compressive loading, IOP Conf. Ser. Mater. Sci. Eng. 1051 (2021) 012016, https://doi.org/10.1088/1757-899X/1051/1/012016.
[28] C.M. Murphy, F.J. O'Brien, Understanding the effect of mean pore size on cell activity in collagen-glycosaminoglycan scaffolds, Cell Adh Migr 4 (2010) 377–381, https://doi.org/10.4161/cam.4.3.11747.
[29] L. Diaz-Gomez, P.D. Kontoyiannis, A.J. Melchiorri, A.G. Mikos, Three-Dimensional printing of tissue engineering scaffolds with horizontal pore and composition gradients, Tissue Eng Part C Methods 25 (2019) 411–420, https://doi.org/10.1089/ten.tec.2019.0112.
[30] D.J. Dickson, R.L. Ely, Silica sol-gel encapsulation of cyanobacteria: lessons for academic and applied research, Appl. Microbiol. Biotechnol. 97 (2013) 1809–1819, https://doi.org/10.1007/s00253-012-4686-8.
[31] L. Diaz-Gomez, P.D. Kontoyiannis, A.J. Melchiorri, A.G. Mikos, Three-Dimensional printing of tissue engineering scaffolds with horizontal pore and composition gradients, Tissue Eng Part C Methods 25 (2019) 411–420, https://doi.org/10.1089/ten.tec.2019.0112.
[32] M. Farzan, R. Roth, J. Schoelkopf, J. Huwyler, M. Puchkov, The processes behind drug loading and release in porous drug delivery systems, Eur. J. Pharm. Biopharm. 189 (2023) 133–151, https://doi.org/10.1016/j.ejpb.2023.05.019.
[33] P. Schneider, Adsorption isotherms of microporous-mesoporous solids revisited, Appl. Catal. Gen. 129 (1995) 157–165, https://doi.org/10.1016/0926-860X(95)00110-7.
[34] R.A. Perez, A. El-Fiqi, J.-H. Park, T.-H. Kim, J.-H. Kim, H.-W. Kim, Therapeutic bioactive microcarriers: Co-delivery of growth factors and stem cells for bone tissue engineering, Acta Biomater. 10 (2014) 520–530, https://doi.org/10.1016/j.actbio.2013.09.042.
[35] J. Tu, A.L. Boyle, H. Friedrich, P.H.H. Bomans, J. Bussmann, N.A.J.M. Sommerdijk, W. Jiskoot, A. Kros, Mesoporous silica nanoparticles with large pores for the encapsulation and release of proteins, ACS Appl. Mater. Interfaces 8 (2016) 32211–32219, https://doi.org/10.1021/acsami.6b11324.
[36] P. Horcajada, A. Rámila, J. Pérez-Pariente, M. Vallet-Regí, Influence of pore size of MCM-41 matrices on drug delivery rate, Microporous Mesoporous Mater. 68 (2004) 105–109, https://doi.org/10.1016/j.micromeso.2003.12.012.
[37] M. Vallet-Regí, F. Balas, M. Colilla, M. Manzano, Bone-regenerative bioceramic implants with drug and protein controlled delivery capability, Prog. Solid State Chem. 36 (2008) 163–191, https://doi.org/10.1016/j.progsolidstchem.2007.10.002.
[38] J. Tu, A.L. Boyle, H. Friedrich, P.H.H. Bomans, J. Bussmann, N.A.J.M. Sommerdijk, W. Jiskoot, A. Kros, Mesoporous silica nanoparticles with large pores for the encapsulation and release of proteins, ACS Appl. Mater. Interfaces 8 (2016) 32211–32219, https://doi.org/10.1021/acsami.6b11324.
[39] T. Limongi, F. Susa, M. Allione, E. Di Fabrizio, Drug delivery applications of three-dimensional printed (3DP) mesoporous scaffolds, Pharmaceutics 12 (2020) 1–18, https://doi.org/10.3390/pharmaceutics12090851.
[40] G.J. Owens, R.K. Singh, F. Foroutan, M. Alqaysi, C.-M. Han, C. Mahapatra, H.-W. Kim, J.C. Knowles, Sol–gel based materials for biomedical applications, Prog. Mater. Sci. 77 (2016) 1–79, https://doi.org/10.1016/j.pmatsci.2015.12.001.
[41] Z. Miri, H.J. Haugen, D. Loca, F. Rossi, G. Perale, A. Moghanian, Q. Ma, Review on the strategies to improve the mechanical strength of highly porous bone bioceramic scaffolds, J. Eur. Ceram. Soc. 44 (2024) 23–42, https://doi.org/10.1016/j.jeurceramsoc.2023.09.003.
[42] J. López-García, M. Lehocký, P. Humpolíček, P. Sáha, HaCaT keratinocytes response on antimicrobial atelocollagen substrates: extent of cytotoxicity, cell viability and proliferation, J. Funct. Biomater. 5 (2014) 43–57, https://doi.org/10.3390/jfb5020043.
[43] S.H. Hristova, A.M. Zhivkov, Isoelectric point of free and adsorbed cytochrome c determined by various methods, Colloids Surf. B Biointerfaces 174 (2019) 87–94, https://doi.org/10.1016/j.colsurfb.2018.10.080.
[44] A. Gamero-Quijano, F. Huerta, E. Morallón, F. Montilla, Modulation of the silica sol-gel composition for the promotion of direct electron transfer to encapsulated cytochrome c, Langmuir 30 (2014) 10531–10538, https://doi.org/10.1021/la5023517.
[45] M. Barisik, S. Atalay, A. Beskok, S. Qian, Size dependent surface charge properties of silica nanoparticles, J. Phys. Chem. C 118 (2014) 1836–1842, https://doi.org/10.1021/jp410536n.
[46] T. Huang, Z. Sun, D.E. Heath, N. O'Brien-Simpson, A.J. O'Connor, 3D printed and smart alginate wound dressings with pH-responsive drug and nanoparticle release, Chem. Eng. J. 492 (2024) 152117, https://doi.org/10.1016/j.cej.2024.152117.
[47] M. Asadi, Z. Salehi, M. Akrami, M. Hosseinpour, S. Jockenhövel, S. Ghazanfari, 3D printed pH-responsive tablets containing N-acetylglucosamine-loaded methylcellulose hydrogel for colon drug delivery applications, Int J Pharm 645 (2023) 123366, https://doi.org/10.1016/j.ijpharm.2023.123366.
[48] T. Yoneda, M. Hiasa, Y. Nagata, T. Okui, F.A. White, Acidic microenvironment and bone pain in cancer-colonized bone, BoneKEy Rep. 4 (2015) 1–9, https://doi.org/10.1038/bonekey.2015.58.
[49] G. Raffaini, M. Catauro, Surface interactions between ketoprofen and silica-based biomaterials as drug delivery system synthesized via sol–gel: a molecular dynamics study, Materials 15 (2022) 2759, https://doi.org/10.3390/ma15082759.
[50] V. Petrelli, M.M. Dell'Anna, P. Mastrorilli, V. Viola, M. Catauro, A. D'Angelo, Synthesis by sol–gel route of organic–inorganic hybrid material: chemical characterization and in vitro release study, Appl. Sci. 13 (2023) 8410, https://doi.org/10.3390/app13148410.